

Research Article

Millimeter-Wave Broadband MIMO Antenna Using Metasurfaces for 5G Cellular Networks

Thanh Nghia Cao,¹ Minh Tam Nguyen,¹ Huu Lam Phan,¹ Duc Dung Nguyen,²
Dinh Lam Vu,³ Thi Quynh Hoa Nguyen ^{1,4} and Jung-Mu Kim ⁴

¹School of Engineering and Technology, Vinh University, 182 Le Duan, Vinh, Vietnam

²Department of Information and Telecommunication Engineering, Soongsil University, 369 Sang-doro, Seoul, Republic of Korea

³Graduate University of Science and Technology, Vietnam Academy of Science and Technology, 18 Hoang Quoc Viet Street, Ha Noi, Vietnam

⁴Department of Electronic Engineering, Jeonbuk National University, Jeonju 54896, Republic of Korea

Correspondence should be addressed to Thi Quynh Hoa Nguyen; ntqhoa@vinhuni.edu.vn
and Jung-Mu Kim; jungmukim@jbnu.ac.kr

Received 28 November 2022; Revised 4 January 2023; Accepted 9 January 2023; Published 8 February 2023

Academic Editor: Chow-Yen-Desmond Sim

Copyright © 2023 Thanh Nghia Cao et al. This is an open access article distributed under the Creative Commons Attribution License, which permits unrestricted use, distribution, and reproduction in any medium, provided the original work is properly cited.

Developing a millimeter-wave (mm-wave) antenna that enables wide bandwidth with its operating band covering the entire global 5G spectrum is highly desirable but very challenging for achieving both compact size and high-performance antenna. Herein, the mm-wave microstrip patch antenna (MPA) and its multiple-input multiple-output (MIMO) configuration based on the metasurfaces for 5G system applications are proposed and investigated by the simulation method. To improve performance and keep the low-profile and low-cost MPA antenna, square ring resonator (SQRR) metasurface and radiating patch are printed on a single dielectric layer. With the presence of the metasurfaces that acting as a secondary radiator, the performance of the designed antenna is significantly improved with a wide operating band in the range of 23.9-30.7 GHz, high peak gain of 9.4 dBic, and radiation efficiency of above 87%. Based on this design, four-port MIMO antenna configuration is performed for evaluating a MIMO system that realizes the advantage features such as compact size, wide bandwidth covering the entire global mm-wave 5G spectrum band of 24.25-29.5 GHz, and excellent diversity performance characterized by good isolation between the adjacent elements and low envelope correlation coefficient. Thus, the MIMO antenna design is a very promising candidate for 5G MIMO mm-wave applications, specifically in cellular systems.

1. Introduction

In recent years, the 5G millimeter-wave (mm-wave) systems are fast-growing fields in wireless communication systems that can support extreme capacity and blazing-fast data speeds to meet the needs of emerging technologies such as mobile ecosystems, autonomous vehicles, and smart cities. The 5G mm-wave networks have been deployed in some regions of the world (US, Japan, Europe, Korea, China, etc.) in the range from 24.25 to 29.5 GHz [1, 2]. Besides, a multiple-input multiple-output (MIMO) system has been identified as an important enabling technology for future 5G communication applications, allowing simultaneous use

of multiple antennas, and thus obtaining higher data rates and greater channel capacity [3]. Therefore, the developing mm-wave MIMO antenna has attracted significant attention for 5G network applications.

However, the design of a compact MIMO antenna is a huge challenge due to the close arrangement of antenna elements that causes the enhancement of isolation between elements and deterioration of the overall performance of the multiple antenna system. Some approaches have been reported to reduce the mutual coupling for MIMO antennas by attenuating and blocking the surface current flow such as defected ground structures, decoupling networks, neutralization lines, parasitic elements, and electromagnetic bandgap

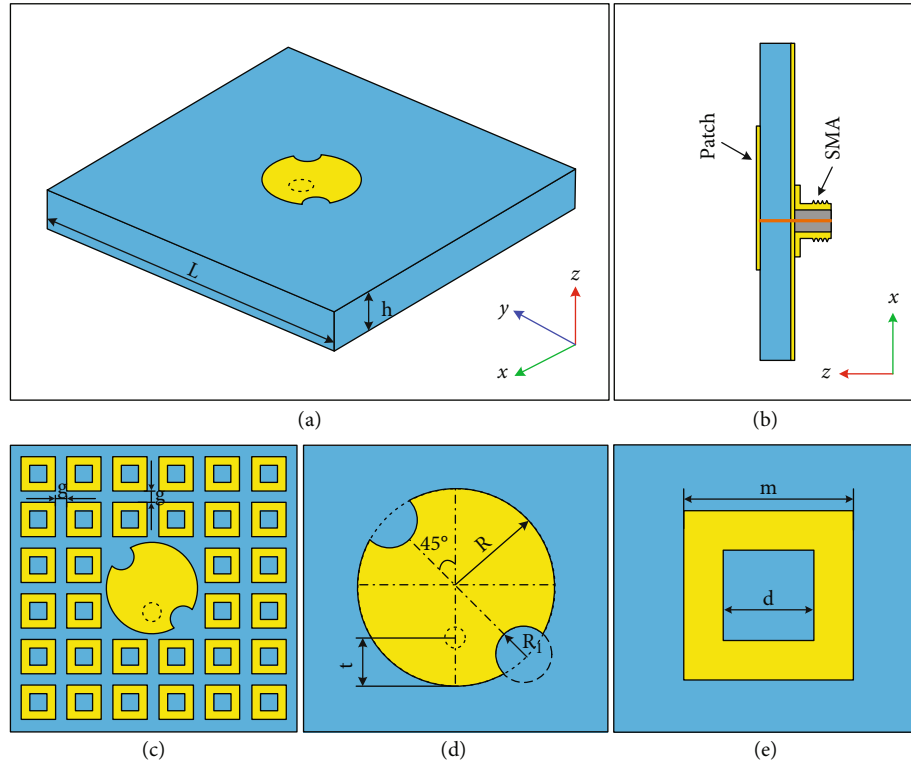


FIGURE 1: Geometry of the proposed four-port MIMO antenna with metasurfaces: (a) top-view and (b) side-view.

TABLE 1: Optimized parameters of the proposed single and MIMO antenna.

Parameter	L	h	R	t	R_1	g	m	d	P	K
Value (mm)	12	0.51	2	0.9	0.75	0.36	1.58	0.75	19.76	7.76

structures [4–7]. Furthermore, MIMO antenna designs require a high gain to deal with the high propagation and atmospheric losses in mm-waves and large enough bandwidth for concurrent functioning [6].

Metasurface is a two-dimensional array of periodic or nonperiodic structures that can manipulate the electromagnetic (EM) waves at the subwavelength scale [8–10]. Due to the exotic features, an appropriate combination of metasurfaces has been found to enhance the MIMO antenna performances such as isolation, gain, and bandwidth. For example, by placing a metasurface above or below of patch resonator, the antenna performance has been reported to enhance markedly [2, 11, 12, 13, 14, 15, 23]. The mechanism for enhancement of the antenna performance is due to the formation of surface wave resonance that creates surface wave propagation along the metasurface for extra resonance [2]. However, these designs use multilayered structures, leading to high-profile, fabrication complexity, and cost. Therefore, the printing of metasurface structures on the top patch resonator and/or bottom ground plane is developed to enhance the antenna performance without increasing its profile [16–18]. Li et al. reported a broad-bandwidth and high-gain patch antenna using planar-patterned metamater-

ial concept operating in the range of 5.3–8.5 GHz [16]. Furthermore, Liang et al. developed a novel single-layer metasurface antenna for wideband operation in the frequency range of 5.11–6.12 GHz [17]. Most of these studies have successfully designed wideband antennas operated at the microwave. More recently, Hussain et al. proposed the metasurface-based single-layer broadband MIMO antenna covering the frequency range of 25–29.5 GHz with good radiation characteristics and excellent diversity performance [18], but its bandwidth is not enough wide to cover the global mm-wave 5G spectrum in the range of 24.24–29.5 GHz.

In this study, we proposed a facile approach to the design of mm-wave broadband MIMO antenna by synergistic benefits-driven through the merger of metasurface and patch resonator of microstrip patch antenna (MPA) structure on a single dielectric layer that can use the advantages of low-profile and low-cost MPA structure and the ability to improve the gain and enlarge bandwidth of metasurface structures. Based on this combination, the proposed antenna has a compact size and high performance that exhibits the operating frequency band in the wide range of 23.9–30.6 GHz covering the entire global mm-wave 5G spectrum.

2. Antenna Design

This section describes the antenna design from single antenna without and with metasurfaces to a four-port MIMO antenna. In these design, substrate material of Roger

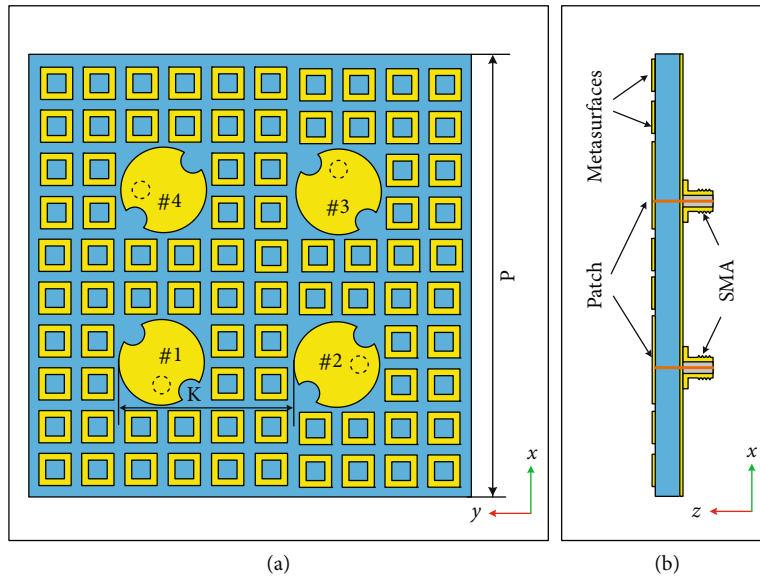


FIGURE 2: Geometry of the proposed four-port MIMO antenna with metasurfaces: (a) top-view and (b) side-view.

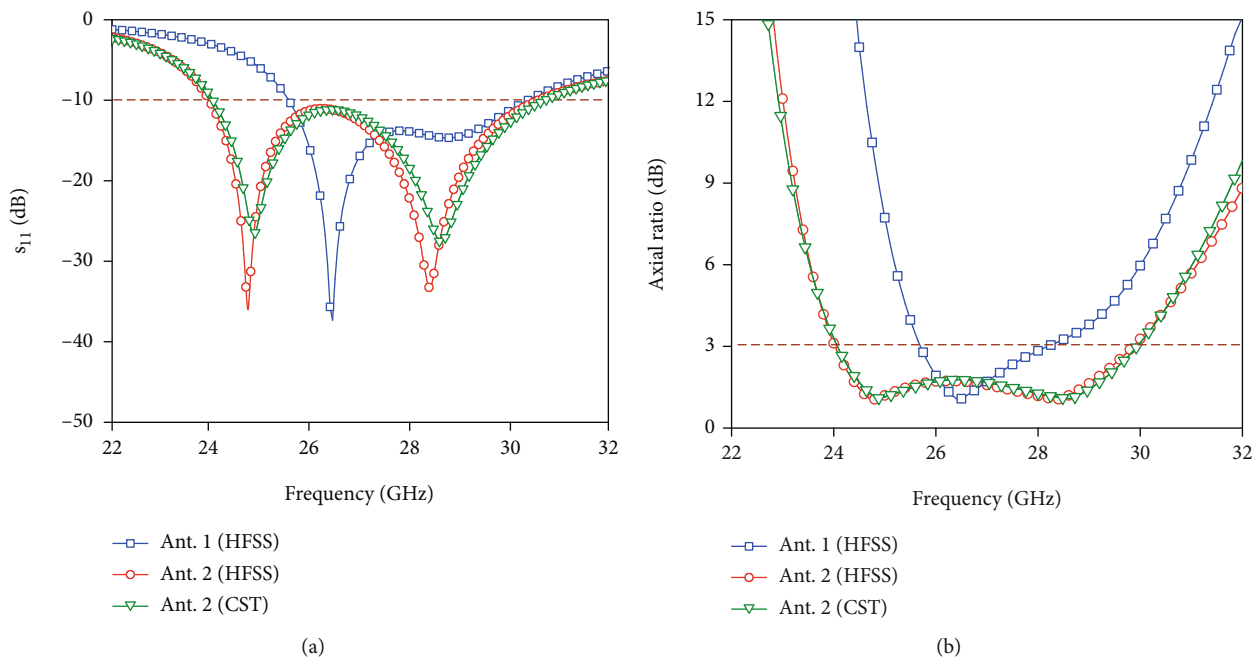


FIGURE 3: (a) S -parameter $|S_{11}|$. (b) Axial ratio of the proposal antenna.

5880LZ with dielectric constant (ϵ) of 2.0, loss tangent ($\tan \delta$) of 0.0009, and a height (h) of 0.8 mm has been used to design the antennas. The aim of this work is to design the antenna that can operate in the entire global mm-wave 5G with simple structure and compact size.

To aid the design and optimization of the proposed antenna, the Ansoft High Frequency Structure Simulator (HFSS) software is used which is based on the finite element method (FEM). For HFSS simulation, the driven modal solution type with maximum delta S of 0.02 and wave-port excita-

tion is used. It is known that in the Computer Simulation Technology (CST), the time domain solver uses finite integration (FIT) technique which is good for wide bandwidth simulation. Therefore, the CST microwave studio software is also carried out to verify the reliability of the obtained results. In this simulation, the open boundary conditions are applied in the x , y , and z directions, and the antenna is fed by waveguide port. It reported the good agreement between both HFSS and CST simulations and experimental results of antennas; therefore, these simulation methods are used in this work.

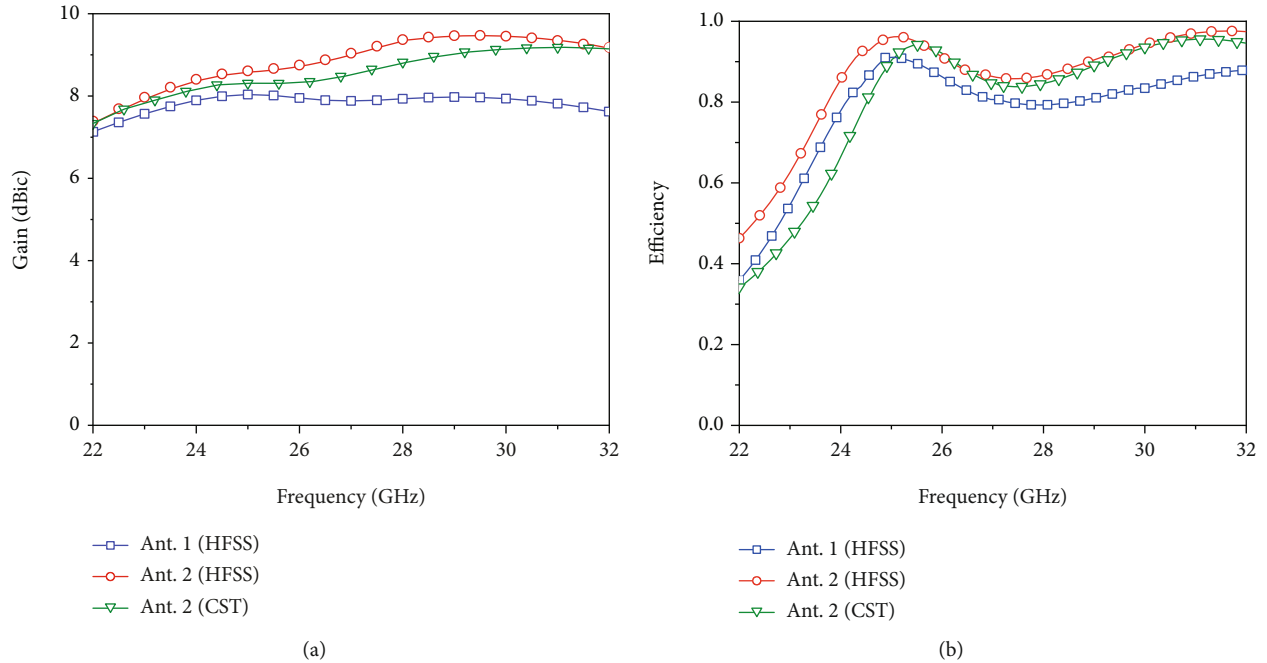


FIGURE 4: (a) Gain and (b) radiation efficiencies of the proposed antenna.

2.1. Single Antenna. The single antenna is initially designed using an MPA structure due to its advantages such as compact, simple to manufacture, and easy integration into the circuit board [19]. The structure of the proposed antenna is shown in Figure 1. The initial circular patch antenna of 28 GHz is calculated using the well-known formula [20]. It was reported that the etching of the slots in the diagonal corners of the antenna patch can improve the impedance bandwidth [21]. Therefore, in the antenna design, the circle patch is etched by two equal circle shapes in the diagonal patch printed on Roger substrate backed with a continuous copper ground plane, as shown in Figure 1(a) (referred to as Ant. 1). The patch resonator is fed by 50Ω coaxial probe (Figure 1(b)). The use of metasurfaces was proposed for enlarging operation bandwidth and improve antenna performance [22]. To design the compact antenna, the metasurface of square ring resonators (SQRRs) is periodically loaded on the top plane of the designed antenna (Figure 1(c), referred to as Ant. 2). The patch resonator and unit cell of metasurface along with the design parameters are shown in Figures 1(d) and 1(e), respectively. The design in this work is aimed for the antenna that can work in the global 5G mm-wave spectrum covering in the range from 24.25 GHz to 29.5 GHz [1, 2]. Therefore, the designed antenna parameters are optimized to operate in the frequency range. The antenna parameters for the optimum performance are shown in Table 1.

2.2. MIMO Antenna. The single antenna using metasurface is arranged into a four-element MIMO array with an overall dimension of the Roger Printed Circuit Board (PCB) of $19.76\text{ mm} \times 19.76\text{ mm}$ while the size of elements and metasurface unit cells is fixed as the proposed single antenna, as shown in Figure 2. To obtain fewer coupling effects, the

MIMO antenna configuration was constructed that the patch resonator elements were at a 90° distance from each other. Each MIMO element consists of an antenna array obtained previously design and is positioned to overlap each other on a single substrate in order to reduce its overall dimension (Figure 2(a)). Such MIMO antenna, the distance between the two neighbor patch resonator elements is 7.76 mm. The feed position and feed method of each element are kept the same as a previously single antenna design as shown in Figure 2(b).

3. Results and Discussion

In this section, the performance results of the designed antennas, including the single antenna without and with metasurfaces and MIMO antenna, are presented in the following subsections. The distinctive characteristics, including suitable operating band, large relative bandwidth, high gain and efficiency, and good isolation between adjacent antenna elements, indicate the potential of the designed antenna.

3.1. Single Antenna. The performance of proposed antenna is evaluated in terms of the reflection coefficient and axial ratio characteristics, gain and radiation efficiency, and radiation pattern in the operating frequency range.

3.1.1. S-Parameter and Axial Ratio. Figure 3 presents the reflection coefficient and axial ratio (AR) of the designed single antennas with and without metasurfaces. As shown in Figure 3(a), by introducing metamaterials, the operating band of antenna obtained from the reflection coefficient ($|S_{11}|$) below -10 dB is expanded from 25.6-30.5 GHz to 23.9-30.7 GHz. Thus, the fractional bandwidth of antenna with metasurfaces of 25% with respect to the central

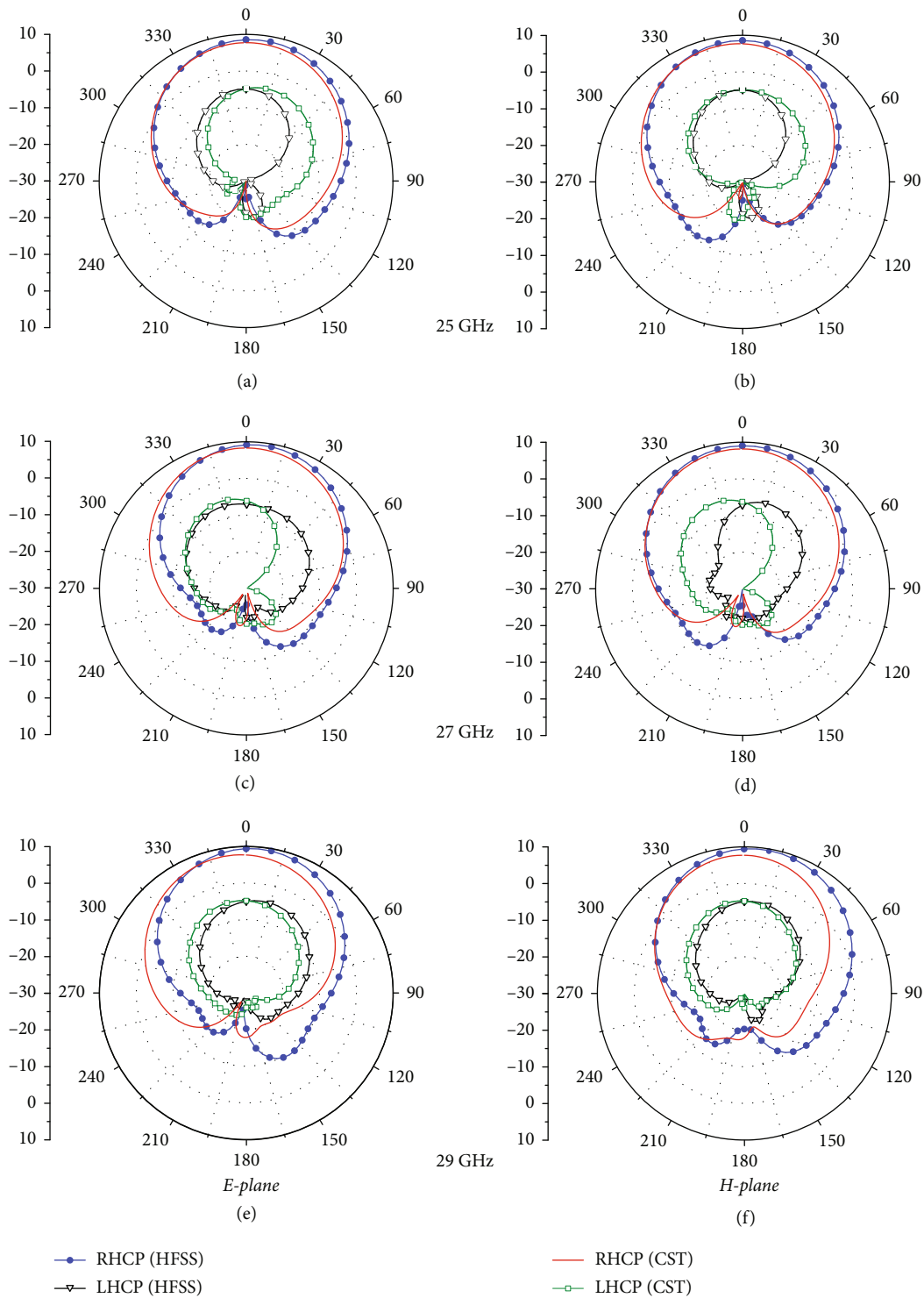


FIGURE 5: Radiation patterns of the proposed antenna with metasurfaces in (a, c, e) *E*-plane and (b, d, f) *H*-plane at various frequencies of 25 GHz, 27 GHz, and 29 GHz, respectively.

frequency is wider than that of the conventional MPA antenna of 17%. Moreover, using metasurface can significantly improve the 3 dB AR bandwidth of the antenna as depicted in Figure 3(b). The 3 dB AR bandwidth of antennas with and without metasurfaces is 21.9% covering 24-

29.9 GHz frequency band and 9.7% covering the 25.6-28.2 GHz frequency band, respectively. To verify the performance of the designed antenna with metasurface, the same antenna is redesigned using CST software. It can be observed that both simulation results using HFSS and CST are

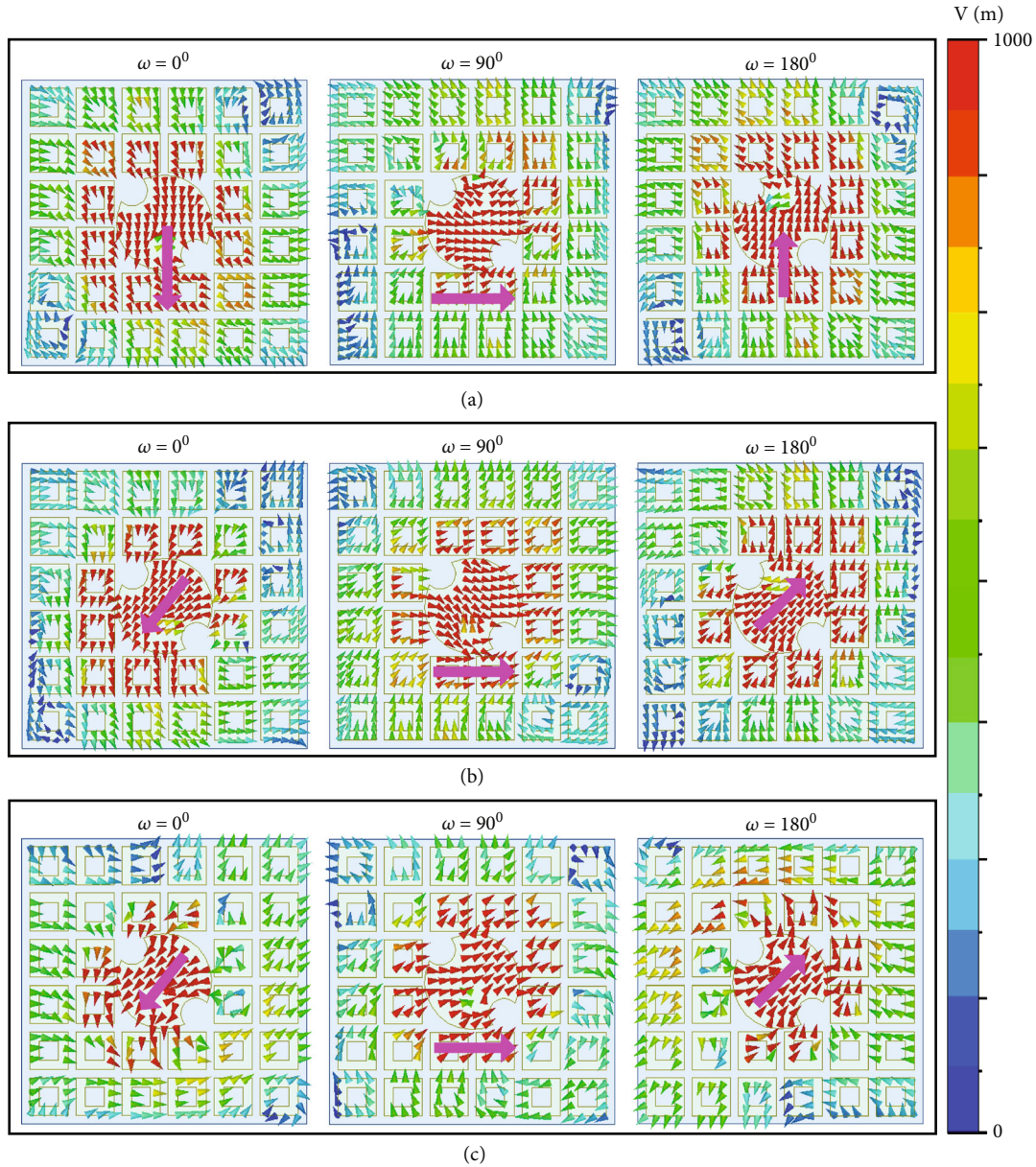


FIGURE 6: Rotation of E -field with the phases of 0° , 90° , and 180° at various frequencies of (a) 25 GHz, (b) 27 GHz, and (c) 29 GHz.

interpreted correctly. These obtained results indicate that the designed single antenna with metasurface achieves the wide-band characteristics, and its operating band is suitable with the entire global 5G mm-wave spectrum.

3.1.2. Gain and Radiation Efficiencies. The gain and antenna's efficiencies are given in Figures 4(a) and 4(b), respectively. It is clear that both gain and radiation efficiencies of the antenna with metasurface are higher than those of antenna without metasurface throughout the operating band because the metasurfaces can act as a secondary radiator for useful extra resources [18]. In the operating band of 23.9–30.7 GHz, the gain of the designed antenna with metasurface keeps above 8.2 dBic. The maximum gain of antennas with

and without metasurface is 9.4 dBic and 8 dBic, respectively. And the efficiency of antennas with and without metasurface is higher than 86% and 78% within the whole operating band, respectively. Meanwhile, there is a slight difference between CST and HFSS simulated results. These observations prove the high performance of the proposed antenna by loading metasurfaces.

3.1.3. Radiation Patterns. The radiation patterns in both principal planes (E and H -planes) at 25, 27, and 29 GHz of the designed antenna with metasurfaces are plotted in Figure 5. Good agreement between simulated CST and HFSS radiation patterns can be observed in both planes. In two planes, the designed antenna exhibits nearly symmetrical

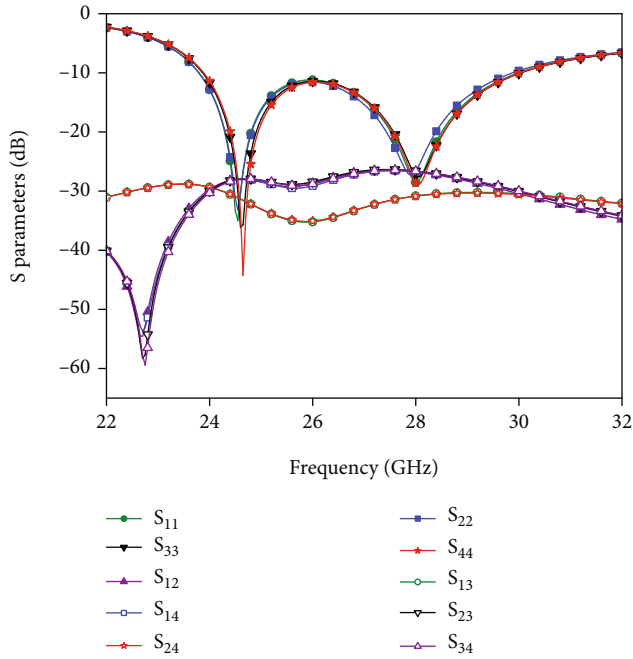


FIGURE 7: Scattering coefficients of the proposed MIMO antenna.

radiation patterns with low side-lobe and back-lobe levels at all frequencies of 25, 27, and 29 GHz. Furthermore, at $\theta = 0^\circ$, the magnitude of Right Hand Circular Polarization (RHCP) is higher than that of Left Hand Circular Polarization (LHCP), indicating that the designed antenna has the RHCP characteristic in its operating band [23].

Moreover, the polarization of the proposed antenna is confirmed by investigating the distribution of the E -field at various frequencies of 25 GHz, 27 GHz, and 29 GHz. Figure 6 presents the E -field distributions for various phases ($\omega = 0^\circ, 90^\circ, \text{ and } 180^\circ$). It shows that the E -field distributions rotate in a counter-clockwise direction with the change of phases ($0^\circ, 90^\circ, \text{ and } 180^\circ$), which demonstrates the RHCP of the proposed antenna [2, 24].

3.2. MIMO Antenna Performance. The performance of four-port MIMO antenna is evaluated based on the S -parameters, envelope correlation coefficient (ECC), diversity gain (DG), and channel capacity loss (CCL) between the adjacent elements.

3.2.1. S-Parameter. The reflection (S_{ii}) and transmission (S_{ij}) coefficients for all ports of the designed MIMO antenna in the frequency range 22 GHz to 32 GHz are shown in Figure 7. The four elements of the MIMO antenna reveal almost similar reflection coefficient responses. Furthermore, all elements of the MIMO antenna can keep the same operating band with $S_{ii} < -10$ dB as the proposed single antenna. The isolation between the antenna elements is a very important parameter for the MIMO antenna design due to high isolation (low coupling) between the elements that will result in enhanced efficiency of the individual elements and reduced power loss due to coupling [25]. As seen in

Figure 7, transmission characteristics of the MIMO array are below -26 dB in the whole operating band, meaning that the mutual coupling between two adjacent elements of the MIMO array is significantly lower; thus, good isolation among the array elements can be obtained. It was reported that the isolation improvement in the MIMO antenna with the presence of metasurface layer is due to the metasurface elements that act as a decoupling structure [26]. To investigate the role of metasurfaces in isolation improvement of the proposed MIMO, we simulated the current distribution at four different ports, and the result is shown in Figure 8. As seen in Figure 8 the surface current is concentrated at the excited patch and elements of the metasurface that locates around the excited patch, indicating that the strong coupling between the MIMO elements and metasurface rather than between the MIMO elements and the nonexcited patch, leading to the high isolation of the MIMO elements is achieved.

3.2.2. Envelope Correlation Coefficient. The MIMO performance of the antenna is evaluated using the parameter of envelope correlation coefficient (ECC). ECC is used to example the correlation between the radiating elements. The ECC (ρ) between the antenna elements is calculated using the following equation [27, 28].

$$\rho_{ij} = \frac{|S_{ii}^* S_{ij} + S_{ji}^* S_{jj}|^2}{(1 - |S_{ii}|^2) - |S_{ij}|^2 (1 - |S_{ji}|^2) - |S_{jj}|^2}, \quad (1)$$

The ECC ideally must be 0, and in practical applications, and the acceptable limit of ECC is less than 0.5 for an isolated MIMO diversity antenna [29]. Figure 9 presents the ECC of the designed MIMO antenna. The results show a very low value of $\rho < 0.0005$ within the operating range which proves the diversity performance and good isolation of the MIMO elements.

3.2.3. Diversity Gain (DG). Another important parameter for evaluating MIMO system performance is the diversity gain (DG), which defines the effect of the diversity scheme on the radiated power. To achieve good quality and reliability in the MIMO antenna systems, the DG value must be high and nearly 10 dB in the operating frequency range. The DG is calculated using the following equation.

$$DG_{ij} = 10 \sqrt{1 - |\rho_{ij}|^2}. \quad (2)$$

The DG for four elements of the MIMO antennas is shown in Figure 10(a). It can be observed that the DG of the antenna is close to the ideal value of 10 dB in the whole operating range.

3.2.4. Channel Capacity Loss. Channel capacity loss (CCL) is one of critical parameters in MIMO systems, which estimates the maximum limit up to which the message transmission can take place without any loss in the communication channel. The CCL is calculated using

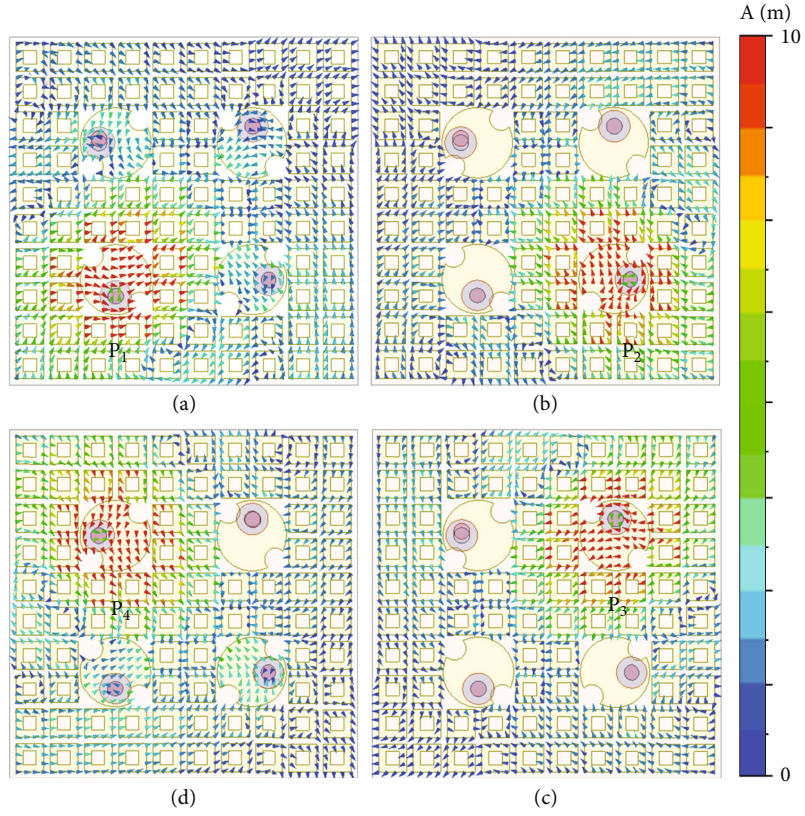


FIGURE 8: Simulated current distribution at different ports of the proposed MIMO antenna.

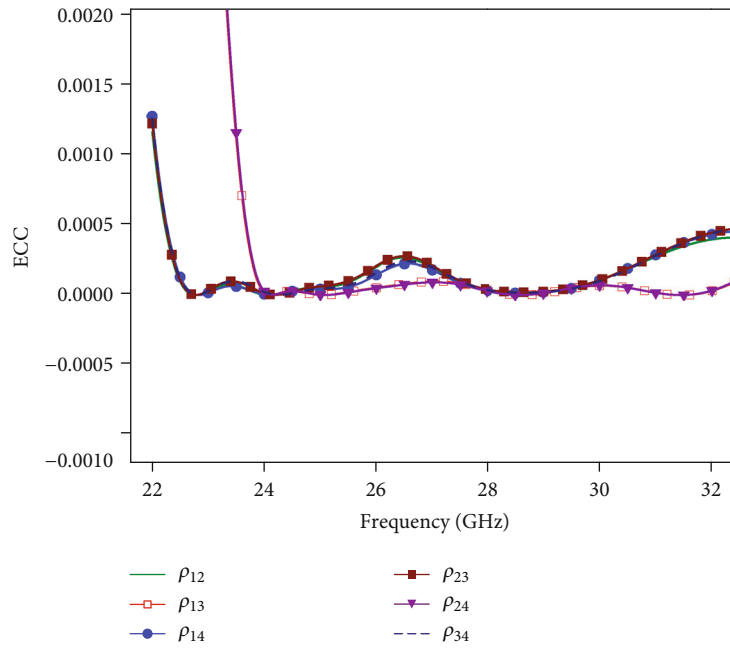


FIGURE 9: ECC of the proposed 4-port MIMO antenna.

equations (3)–(6).

where A_{ij} is the correlation matrix, for $i, j = 1, 2, 3$ and 4 .

$$C_{ij}(\text{loss}) = -\log_2 \det (A_{ij}), \quad (3)$$

$$A_{ij} = \begin{bmatrix} \sigma_{ii} & \sigma_{ij} \\ \sigma_{ji} & \sigma_{jj} \end{bmatrix}. \quad (4)$$

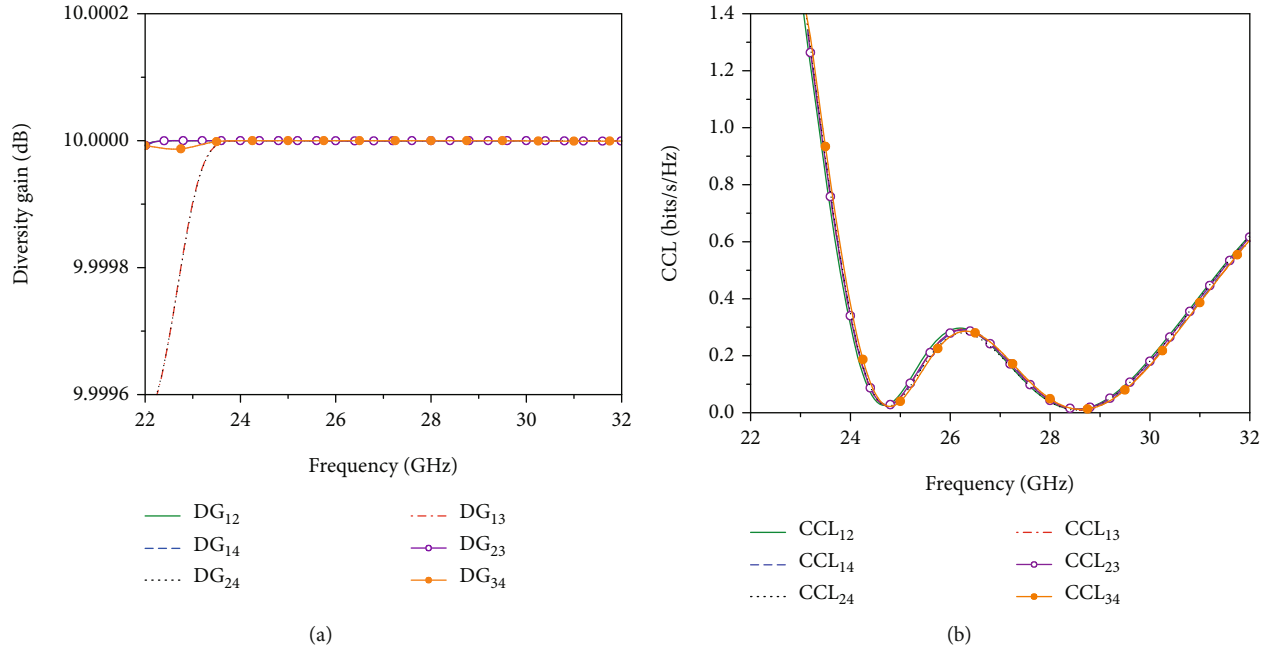


FIGURE 10: (a) DG and (b) CCL of the proposed 4-port MIMO antenna.

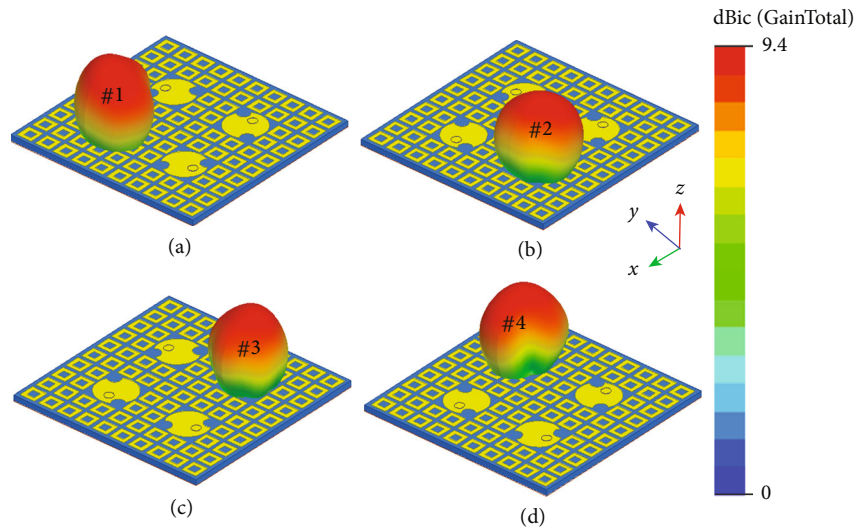


FIGURE 11: 3D radiation patterns of the proposed MIMO antenna at 27 GHz.

The elements of correlation matrix can be obtained by the following equations:

$$\sigma_{ii} = 1 - (|S_{ii}|^2 + |S_{ij}|^2), \quad (5)$$

$$\sigma_{ij} = -|S_{ii}^* S_{ij} + S_{ji} S_{jj}^*|. \quad (6)$$

Figure 10(b) shows CCL for all elements of the MIMO antennas. The acceptable CCL value must be less than 0.4 bits/s/Hz to obtain the high throughput in the antenna system [29]. As seen in Figure 10(b), the CCL of antenna elements of the MIMO systems is below 0.23 bits/s/Hz in the

global mm-wave 5G spectrum of 24.25-29.5 GHz, which proves the proposed MIMO antenna's high throughput.

3.2.5. 3D Radiation Patterns. Figure 11 shows 3D radiation patterns for all elements of the MIMO antennas. The radiation patterns are not changed in MIMO configuration, indicating that the performance of each antenna element is independent of that of other antennas. The maximum gain of antenna elements of the MIMO configuration is 9.4 dBic as seen in Figure 11.

3.3. Performance Comparison. The performance comparison of the proposed MIMO antenna with the existing state-of-the-art mm-wave 5G MIMO antenna in terms of the

TABLE 2: Performance comparison of the proposed designed MIMO antenna with other mm-wave 4-port MIMO antennas.

Refs.	Working band (GHz)	Total size (mm ³)	BW (%)	Max. gain (dBic)	Min. isolation (dB)	ECC	Substrate
[25]	26-31	40 × 31 × 0.254	17.5	10	21	0.0015	Neltec
[6]	25.5-29.6	30 × 35 × 0.76	14.9	8.1	10	0.01	Rogers R04350B
[30]	27-29	30 × 30 × 0.787	7.1	6.1	29	0.16	Rogers 5880
[18]	24.5-31	20.4 × 20.4 × 0.51	23.4	11	30	0.015	Rogers 5880LZ
This work	23.9-30.7	19.76 × 19.76 × 0.51	25	9.4	26	0.0005	Rogers 5880LZ

working frequency band, total size, bandwidth, gain, isolation, ECC, and substrate type is presented in Table 2. As seen in Table 2, the proposed MIMO antenna has the most compact size and the widest bandwidth while achieving a moderate gain and isolation between the antennas.

4. Conclusion

The mm-wave MPA and its 4-port MIMO configuration using metamaterials for 5G applications were proposed and investigated by the simulation method. To improve performance and keep the low-profile and low-cost MPA antenna, the SQRR metasurfaces were printed on the dielectric layer together with the radiating patch, acting as a secondary radiator. Thus, by loading metasurfaces, the MPA antenna achieves a broad bandwidth in the range of 23.9-30.7 GHz with a high peak gain 9.4 dBic and radiation efficiency of above 87%. Based on the high performance of the proposed antenna, a four-port MIMO array was designed and evaluated. The designed MIMO antenna revealed the advantages of features such as compact size, wide bandwidth covering the entire global mm-wave 5G spectrum band of 24.25-29.5 GHz, and excellent diversity performance characterized by good isolation between the adjacent elements and low ECC; thus, this antenna design is a highly desirable candidate for 5G MIMO mm-wave applications, specifically in cellular systems.

Abbreviations

mm-wave: Millimeter-wave
 SQRR: Square ring resonator
 MPA: Microstrip patch antenna.

Data Availability

The data used to support the findings of this study are included within the article.

Conflicts of Interest

The authors declare no conflict of interest.

Acknowledgments

This work was supported by the Vietnamese Ministry of Education and Training, Vietnam (Grant number B2021-TDV-02). The authors are grateful to the supports from the National Research Foundation of Korea (NRF) grant

funded by the Korea government (MSIT) (No. 2021R1A4A1032234).

References

- [1] Qualcomm Technologies, *Spectrum for 4G and 5G*, 2017, Aug. 2019, <https://www.qualcomm.com/news/media-center.2020>.
- [2] N. Hussain, M. J. Jeong, A. Abbas, T. J. Kim, and N. Kim, "A metasurface-based low-profile wideband circularly polarized patch antenna for 5G millimeter-wave systems," *IEEE Access*, vol. 8, pp. 22127–22135, 2020.
- [3] C. X. Wang, F. Haider, X. Gao et al., "Cellular architecture and key technologies for 5G wireless communication networks," *IEEE Communications Magazine*, vol. 52, no. 2, pp. 122–130, 2014.
- [4] I. Nadeem and D. Y. Choi, "Study on mutual coupling reduction technique for MIMO antennas," *IEEE Access*, vol. 7, pp. 563–586, 2019.
- [5] S. F. Jilani and A. Alomainy, "Millimetre-wave T-shaped MIMO antenna with defected ground structures for 5G cellular networks," *IET Microwaves, Antennas & Propagation*, vol. 12, no. 5, pp. 672–677, 2018.
- [6] M. Khalid, S. Iffat Naqvi, N. Hussain et al., "4-port MIMO antenna with defected ground structure for 5G millimeter wave applications," *Electronics*, vol. 9, no. 1, p. 71, 2020.
- [7] M. Khalily, R. Tafazolli, P. Xiao, and A. A. Kishk, "Broadband mm-wave microstrip array antenna with improved radiation characteristics for different 5G applications," *IEEE Transactions on Antennas and Propagation*, vol. 66, no. 9, pp. 4641–4647, 2018.
- [8] C. L. Holloway, E. F. Kuester, J. A. Gordon, J. O'Hara, J. Booth, and D. R. Smith, "An overview of the theory and applications of metasurfaces: the two-dimensional equivalents of metamaterials," *IEEE Antennas and Propagation Magazine*, vol. 54, no. 2, pp. 10–35, 2012.
- [9] M. Faenzi, G. Minatti, D. González-Ovejero et al., "Metasurface antennas: new models, applications and realizations," *Scientific Reports*, vol. 9, no. 1, article 10178, 2019.
- [10] C. Zhang, J. Gao, X. Cao, S. J. Li, H. Yang, and T. Li, "Multi-function tunable metasurface for entire-space electromagnetic wave manipulation," *IEEE Transactions on Antennas and Propagation*, vol. 68, no. 4, pp. 3301–3306, 2020.
- [11] Y. Liu, K. Song, Y. Qi, S. Gu, and X. Zhao, "Investigation of circularly polarized patch antenna with chiral metamaterial," *IEEE Antennas and Wireless Propagation Letters*, vol. 12, pp. 1359–1362, 2013.
- [12] F. Liu, J. Guo, L. Zhao, G. L. Huang, Y. Li, and Y. Yin, "Dual-band metasurface-based decoupling method for two closely packed dual-band antennas," *IEEE Transactions on Antennas and Propagation*, vol. 68, no. 1, pp. 552–557, 2020.

- [13] M. Guo, W. Wang, and P. Huang, "Double-layer metasurface-based low profile broadband X-band microstrip antenna," *IET Microwaves, Antennas & Propagation*, vol. 14, no. 9, pp. 919–927, 2020.
- [14] X. Li, J. Yang, Y. Feng, M. Yang, and M. Huang, "Compact and broadband antenna based on a step-shaped metasurface," *Optics Express*, vol. 25, no. 16, pp. 19023–19033, 2017.
- [15] L. Asadpor, G. Sharifi, and M. Rezvani, "Design of a high-gain wideband antenna using double-layer metasurface," *Microwave and Optical Technology Letters*, vol. 61, no. 4, pp. 1004–1010, 2019.
- [16] L. W. Li, Y. T. S. LiYN, J. R. Mosig, and O. J. F. Martin, "A broadband and high-gain metamaterial microstrip antenna," *Applied Physics Letters*, vol. 96, no. 16, article 164101, 2010.
- [17] Z. Liang, J. Ouyang, and F. Yang, "Low-profile wideband circularly polarised single-layer metasurface antenna," *Electronics Letters*, vol. 54, no. 24, pp. 1362–1364, 2018.
- [18] N. Hussain, M. J. Jeong, A. Abbas, and N. Kim, "Metasurface-based single-layer wideband circularly polarized MIMO antenna for 5G millimeter-wave systems," *IEEE Access*, vol. 8, pp. 130293–130304, 2020.
- [19] M. J. Jeong, N. Hussain, J. W. Park, S. G. Park, S. Y. Rhee, and N. Kim, "Millimeter-wave microstrip patch antenna using vertically coupled split ring metaplate for gain enhancement," *Microwave and Optical Technology Letters*, vol. 61, no. 10, pp. 2360–2365, 2019.
- [20] C. A. Balanis, "Antenna Theory: Analysis and Design," in *3rd ed.*, Wiley Interscience, p. 803, 2005.
- [21] M. M. Hasan, M. T. Islam, M. Samsuzzaman et al., "Gain and isolation enhancement of a wideband MIMO antenna using metasurface for 5G sub-6 GHz communication systems," *Scientific Reports*, vol. 12, no. 1, p. 9433, 2022.
- [22] S. Tariq, S. I. Naqvi, N. Hussain, and Y. Amin, "A metasurface-based MIMO antenna for 5G millimeter-wave applications," *IEEE Access*, vol. 9, pp. 51805–51817, 2021.
- [23] R. Xu, J. Li, Y. X. Qi, Y. Guangwei, and J. J. Yang, "A design of triple-wideband triple-sense circularly polarized square slot antenna," *IEEE Antennas and Wireless Propagation Letters*, vol. 16, pp. 1763–1766, 2017.
- [24] W. Su, J. Li, and R. H. Liu, "A compact double-layer wideband circularly polarized microstrip antenna with parasitic elements," *International Journal of RF and Microwave Computer-Aided Engineering*, vol. 31, no. 1, article e22471, 2021.
- [25] Z. Wani, M. P. Abegaonkar, and S. K. Koul, "A 28-GHz antenna for 5G MIMO applications," *Progress in Electromagnetics Research Letters*, vol. 78, pp. 73–79, 2018.
- [26] N. Hussain, T. D. Pham, and H. H. Tran, "Circularly polarized MIMO antenna with wideband and high isolation characteristics for C-band communication systems," *Micromachines*, vol. 13, no. 11, p. 1894, 2022.
- [27] S. Blanch, J. Romeu, and I. Corbella, "Exact representation of antenna system diversity performance from input parameter description," *Electronics Letters*, vol. 39, no. 9, pp. 705–707, 2003.
- [28] S. H. Chae, O. Sk, and S. O. Park, "Analysis of mutual coupling, correlations, and TARC in WiBro MIMO array antenna," *IEEE Antennas and Wireless Propagation Letters*, vol. 6, pp. 122–125, 2007.
- [29] A. W. M. Saadh, P. Ramaswamy, and T. Ali, "A CPW fed two and four element antenna with reduced mutual coupling between the antenna elements for wireless applications," *Applied Physics A*, vol. 127, no. 2, p. 88, 2021.
- [30] M. M. Kamal, S. Yang, R. Xc et al., "Infinity shell shaped MIMO antenna array for mm-wave 5G applications," *Electronics*, vol. 10, no. 2, p. 165, 2021.